Journal of Institute of Science and Technology, 31(1), 119-136 (2026)
ISSN: 2467-9062 (print), e-ISSN: 2467-9240
https://doi.org/10.3126/jist.v31i1.86921

Research Article

IN SILICO SEARCH OF POTENT PHYTOECDYSTEROIDS TARGETING DIFFERENT CANCER PROTEINS

Nitesh Mallik[1§], Ashish Phuyal[1§], Anuraj Phunyal[1], Narendra Bhatta[1], Amar Waiba[1], Jhashanath Adhikari Subin[2], Achyut Adhikari[1*]

[1] *Central Department of Chemistry, Tribhuvan University, Kirtipur 44618, Kathmandu, Nepal*
[2]*Forest Biomaterials Science and Engineering, Institute of Applied Sciences, Madan Bhandari Institute of Science and Technology, Chitlang Makwanpur, 44100, Nepal*
[*] *Correspondence: achyutraj05@gmail.com*
[§]*These authors contributed equally*

(*Received*: November 28, 2025; *Revised*: February 21, 2026; *Accepted*: May 31, 2026)

ABSTRACT

Cancer remains a major global health challenge, and existing drugs have limited efficacy and adverse side effects. Key molecular regulators such as PARP1, ABL1, and CDK2 represent attractive targets for developing safer and more effective anticancer agents. MDA468 (Breast cancer), HCT-116 (Colon Cancer), CCRF (Leukemia), MDA-MB-435 (Melanoma), HOP-18 (non-small lung cancer), SKOV3 (Ovarian cancer), DU-145(Prostate cancer), and SN12K1 (Renal cancer) are cell lines studied in this paper. 216 phytoecdysteroids were computationally screened against these targets using molecular docking, ADMET profiling, and molecular dynamics simulations (MDS). Among them, *Ecdysterone 22-benzoate 25-O-β-D-glycoside* (PES 1) exhibited strong binding affinities of –11.3 kcal/mol (3L3M) and –9.1 kcal/mol (8H7H), while *E-2-Deoxy-20-hydroxyecdysone 3-[4-(1-β-D-glucopyranosyl)]-caffeate* (PES 44) demonstrated affinities of –9.3 kcal/mol (2A0C) and –9.2 kcal/mol (8H7H). Both complexes maintained RMSD values below 2 Å, and ADMET predictions further indicated favourable pharmacokinetic properties and low predicted toxicity. These findings suggest that PES 1 and PES 44 are promising phytoecdysteroid-based inhibitors with potential anticancer activity, warranting further extended simulations and experimental validation for their development into effective and safer anticancer therapeutics.

Keywords: Binding affinity, Cancer**,** Chemotherapy, Molecular docking, Phytoecdysteroids

INTRODUCTION

Cancer is a significant global health issue, with 19.3 million new cases and 10 million deaths annually (Chhikara & Parang, 2023). It is characterized by the abnormal growth of cells, particularly when tumor cells in the body metastasize (Nussbaumer et al., 2011). Major types of cancer include carcinoma, sarcoma, leukemia, lymphoma, and melanoma, named after the originating cells (Schott et al., 2015). Specific cancers are linked to various cell lines. Cancer cells such as HCT-116, BT-549, HOP-18, and PC-3 are linked to colorectal, breast, lungs, and prostate cancer, respectively (Klijn et al., 2015). Cancer patients typically have the treatment options of surgery, radiotherapy, or chemotherapy, with chemotherapy often being the most viable due to the high costs and low success rates of the other methods. However, chemotherapy faces challenges, like toxicities and drug resistance, that limit its effectiveness (Baskar et al., 2012). Anticancer drugs function by suppressing tumor growth, primarily by interfering with cell division, thereby reducing the number of tumor cells that can proliferate (Malhotra & Perry, 2003). Small molecules are often used to inhibit the plasma membranes of these tumor cells (Hoelder et al., 2012). Most cancer inhibitors target tyrosine protein kinases, particularly ABL1, with Imatinib receiving food and drug administration (FDA) approval in 2001. Other targets include vascular endothelial growth factor (VEGF), poly(ADP-ribose) polymerase 1 (PARP1), human epidermal growth factor receptor 2 (HER2), cyclin-dependent kinase 2 (CDK2), and epidermal growth factor receptor (EGFR) (Seebacher, Stacy, Porter, & Merlot, 2019). The research paper focuses on PARP1, CDK2, and ABL1 inhibitors: PARP1 inhibitors prevent the repair of damaged cancer cells, CDK2 inhibitors disrupt cell cycle progression from the G1 (growth) phase to the S (synthesis) phase, and ABL1 inhibitors hinder DNA repair and synthesis, leading to tumor cell death.

More than 8,000 receptor sites for cancer exist (Brown et al., 2023), and 16 are major targets for drug development. PARP1, EGFR, and ERBB2 classes have been chosen for significant medical research

(Zhou et al., 2020). Notable classes include PARP1, EGFR, and ERBB2, which are the focus of significant medical research. Drugs targeting PARP1 include Niraparib, Olaparib, and Rucaparib, which are powerful poly(ADP-ribose) polymerase (PARP) inhibitors that are authorized to treat malignancies (particularly ovarian) with homologous recombination deficiency (HRD) or BRCA mutations by preventing DNA repair, that results in cell death (synthetic lethality) (Palazzo & Ahel, 2018), while EGFR inhibitors are represented by Trastuzumab, Gefitinib, and Cetuximab are targeted cancer therapies that inhibit different receptors in the HER/ErbB family (Roskoski, 2014). Other targeted receptors include TOP1, which is inhibited by topotecan and irinotecan, and BCL2, targeted by docetaxel (Asghar et al., 2015). This research paper emphasizes the inhibition of PARP1 class (PARP1) and kinase classes, specifically ABL1 and CDK2, with standard drugs such as Olaparib (Palazzo & Ahel, 2018) for PARP1, Imatinib for ABL1 (Raimondi et al., 2014), and Palbociclib for CDK2 (Roskoski, 2016) (Fig. 1).

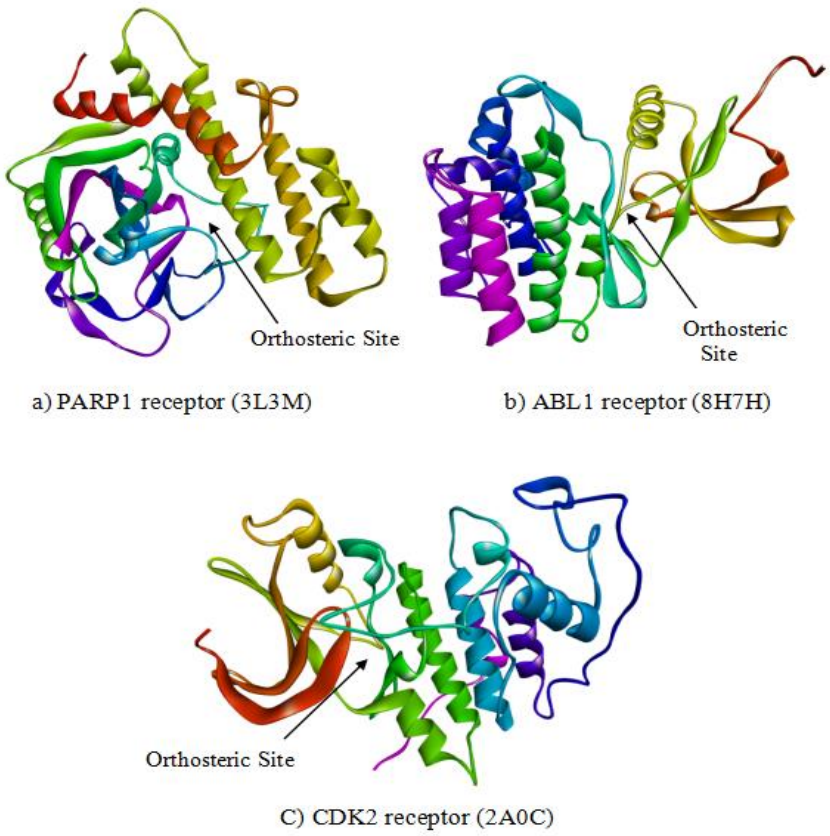

Figure 1. (a) PARP1 receptor (3L3M), (b) ABL1 receptor (8H7H), (c) CDK2 receptor (2A0C)

Medicinal plants have been historically utilized for the treatment of various diseases (Phuyal et al., 2019), particularly cancer, owing to the presence of bioactive secondary metabolites that inhibit cancer cell growth. Among these metabolites, triterpenoids, flavonoids, and glycosides have received considerable attention for their anticancer potential (Chiang et al., 2003). One such group is phytoecdysteroids, a class of plant-derived steroids known for their role in regulating insect moulting and development (Bathori & Pongracz, 2005). Recent studies have revealed the anticancer potential of phytoecdysteroids, which can inhibit the progression of cancer development by acting on specific molecular receptors, including the PARP1, ABL1, and CDK2 receptors (Das et al., 2021).

Thus, the present study proposes an evaluation of the anticancer potential of the identified ligands of the phytoecdysteroid compounds using the molecular docking technique for evaluating the binding affinities of the compounds with the target receptors. In addition, ADMET analysis has been carried out to evaluate the drug-likeness properties of the compounds.

MATERIALS AND METHODS

Selection, preparation, and screening of ligands

Different phytoecdysteroids with reported biological properties were selected as ligands from the literature (Adhikari et al., 2025). Their structure was created in ChemDraw Ultra 12.0. The ligands were then converted into 3D structures by energy minimization

using the Avogadro software (version 1.1) (Hanwell et al., 2012). The PDB format of ligands was further converted to pdbqt format using the AutoDock Tools program (Waiba et al., 2025). Ligands were screened to determine the toxicities of organic molecules with the help of the ProTox-II server, which analyzes many toxicity parameters like hepatotoxicity, carcinogenicity, mutagenicity, cytotoxicity, and immunotoxicity of small molecules (Banerjee et al., 2018).

Receptor preparation and validation

Three anti-cancer receptors (3L3M, 2A0C, and 8H7H) were identified as potential targets. The receptors were downloaded from the www.rcsb.org website in the PDB format (Rose et al., 2017). The three receptors were poly (ADP Ribose) polymerase (PARP1) [PDBID: 3L3M] (Penning et al., 2010), tyrosine-protein kinase (ABL1) [PDBID: 8H7H] (Chen et al., 2023), and cyclin-dependent kinase 2 (CDK2) [PDBID: 2A0C] (Kryštof et al., 2005). 3L3M, 8H7H, and 2A0C have resolutions of 2.50 Å, 2.28 Å, and 1.95 Å, respectively. The X-ray crystal structures of these receptors were processed using the PyMOL software (version 2.5.5) (Schrodinger & Delano, 2020) by removing water, ions, and other ligands, followed by the addition of polar hydrogen. 3D structures of receptors were validated using the SAVESv6.0 web server, which contains three programs, called ERRAT, VERIFY3D, and PROCHECK. ERRAT gives the overall quality factor of the receptor and analyses non-bonded interaction patterns to verify it (Colovos & Yeates, 1993). VERIFY checks the percentage of residues that have 3D-1D values which are greater than or equal to 0.1 (Bowie et al., 1991). The 3D-1D value in protein structure assessment refers to the compatibility of an atomic model's three-dimensional (3D) structure with its amino acid sequence (1D). PROCHECK analyses receptor stereochemical quality like the Ramachandran plot (Laskowski, MacArthur, Moss, & Thornton, 1993). A Ramachandran plot is a biochemistry tool that visualizes the energetically acceptable regions for backbone dihedral angles in protein structures, aiding in determining the most beneficial combinations for protein stability and understanding protein shape and stability (Laskowski et al., 2012). There were missing residues in the 2A0C and 8H7H receptor sequences. Their missing residues were filled with the SWISS-MODEL server (Waterhouse et al., 2018), which is based on the open structure strategy of the computational structural biology framework (Biasini et al., 2014). A FASTA sequence was downloaded from the RCSB website and employed the BLAST (Altschul et al., 1997) database search technique, which generates templates. A template having the highest Global Model Quality Estimation (GMQE) (Biasini et al., 2013) and identity percentage was selected for building 3D models. 2F4J.1.A and 2A0C.1.A were selected to build model for 8H7H and 2A0C, respectively. A model was downloaded in protein data bank (PDB) format, which was cleaned and then converted into pdbqt format. AutoDock Tools (version 1.5.7) (Trott & Olson, 2010) was used to clean by removing ligands and water molecules, followed by the addition of polar hydrogen atoms. Kollmann charges of 10.0, -70.016, and 14.0 were added into 3L3M, 8H7H, and 2A0C, respectively, and were ready to dock with ligands.

Protocol validation

Protocol validation means ensuring the whole process (Karki et al., 2024). The root mean square deviation (RMSD) between the native ligand and the hit ligands (best candidates from molecular docking) was calculated. RMSD of 3L3M, ABL1, and CDK2 receptors were 1.81 Å, 2.43 Å, and 2.29 Å. RMSD of all three receptors with hit molecules was less than 2 Å, which is acceptable.

Molecular docking and scoring

Molecular docking was done between non-toxic ligands and a clean target receptor with the AutoDock Vina (version 1.5.7) program (Trott & Olson, 2010). Each docking program employs a distinct search strategy, utilizing its own internal conformational search algorithm; for example, AutoDock Vina uses a gradient-based optimization approach (Table 1). Receptor-ligand visualization was done with Biovia Discovery Studio 2021 Client software.

Table 1. Methods for docking

PDB ID	Grid box size (Å)	Grid box centre (x,y,z)	Exhaustiveness	Number of modes	Energy range
3L3M	40×40×40	26.36, 11.22, 27.02	32	20	4
8H7H		1.99, -7.50, -24.57			
2A0C		-0.03, 6.63, 26.81			

In silico predictive cancer cell line inhibition study by the pdCSM server

Small molecules' anticancer inhibition activity can be studied by using a graph-based signature, which is a representation of the chemical structure of tiny molecules using a pdCSM server. It accurately predicts molecules that are likely to inhibit one or more cancer cell lines. Their quantitative structure-activity association, along with machine learning models, predicts molecular pharmacodynamics and bioactivity of compounds with anticancer capabilities against diverse cell types. There are many types of cancer cell lines for which it can be predicted accurately. The ligand's anticancer activity against cancer cell lines was evaluated with Pearson's correlation coefficients of up to 0.74. The anticancer activity of the cell lines was expressed in µM. The values greater than or equal to 5.0 were active against that cancer cell line. MDA-MB-468 (Breast cancer), HCT-116 (Colon Cancer), CCRF (Leukaemia), MDA-MB-435 (Melanoma), HOP-18 (non-small lungs cancer), SK-OV-3 (Ovarian cancer), DU-145(Prostate cancer), and SN12K1 (Renal cancer) are some cancer cell lines predicted by pdCSM. Different cancer cell line inhibition is calculated based on machine learning of experimental data correlation with a graph-based signature of small molecules (Al-Jarf et al., 2021).

In-silico predictive CDK2 inhibition study by the kinCSM server

Cyclin-dependent kinase (CDK2) is a special type of kinase protein that inhibits cancer cells, acting as an on/off switch in various cellular signalling pathways and regulating tumor and cancer proteins (Philipp-Staheli et al., 2001). This is accomplished with the use of the kinCSM server, an integrative computational tool that can precisely identify an efficient inhibitor of cyclin-dependent kinase by predicting protein ligand-kinase inhibition constants (pKi). The prediction models record the physicochemical and geometric features of tiny test molecules. It predicts the ligand binding site on the protein. It predicts whether the ligand binds at the orthosteric site or the allosteric site. It also classifies the type of CDK2 inhibitors into type I, type II, and type I1/2. Type I inhibitors bind to the active site of the kinase and compete with ATP (adenosine triphosphate) for binding and are frequently ATP-competitive. Type II inhibitors are more prevalent and extensively studied. Type II inhibitors stabilize the inactive conformation of a kinase by binding to an allosteric site near the active site. Type I1/2 Inhibitors are hybrids combining characteristics of both Type I and Type II inhibitors, and interact with active and allosteric sites. CDK2 inhibitors were accurately identified with Matthew's Correlation Coefficients of up to 0.74, and inhibition constants predicted with Pearson's correlation of up to 0.76. The server predicts the CDK2 ligand binding (pKi) values. The ligand binding (pKi) values greater than or equal to 5.00 are considered to inhibit the CDK2 protein.

RESULTS AND DISCUSSION

Selection, preparation, and screening of ligands

Out of 216 phytoecdysteroid ligands, 44 ligands (Table S1, Fig. S1) were screened, and five ligands were inactive for hepatotoxicity, carcinogenicity, immunotoxicity, mutagenicity, and cytotoxicity, whereas 39 of the ligands were inactive in all except immunotoxicity, where they were active (Table S3). These 44 ligands were classified as class 4 compounds. Class 4 compounds are harmful if swallowed ($300 < LD50 \leq 2000$) according to the globally harmonized system of classification (GHS). Though toxic in one parameter, they were still selected for molecular docking (Khatiwada et al., 2025).

Protein preparation and target validation

Structures of PARP1, ABL1, and CDK2 receptors were prepared and then validated with the SAVESv6.0 server. ERRAT module provides the receptor's overall quality factor and examines the non-bonded interaction pattern to confirm it (Karki et al., 2024). The overall quality factors of the three receptors were 92.35%, 98.35%, and 95.37%, respectively. The VERIFY module evaluates the percentage of residues with 3D–1D profile scores $\geq$ 0.1; the corresponding values for the receptors were 93.68%, 79.81%, and 82.65%, confirming acceptable 3D–1D compatibility. PROCHECK module analyses receptor stereochemical quality. The PROCHECK module of these receptors was used to extract the Ramachandran plot (Table S2, Fig. S2, Fig. S4), which is a plot of Phi and Psi angles in a polypeptide. These angles visualize the energetically favored region of residues in the receptor structure, and help to know about conformational regions available to the receptor backbone.

Molecular docking analysis

Molecular docking was performed using Auto Dock Vina for 44 phytoecdysteroids. The binding affinity scores of the selected phytoecdysteroids, native

compounds, and reference drugs with PDB ID: 3L3M, 2A0C, and 8H7H (Table 2). The binding affinities of the PARP1 receptor (3L3M) were between -11.3 and -9.0 kcal mol^{-1}. The binding affinity of the reference ligand for the PARP1 receptor (3L3M) was -10.1, whereas binding affinities of the reference drugs were -10.3 and -10.8 kcal mol^{-1}. The binding affinity of PES 1, PES 2, PES 3, PES 4, and PES 5 was lower than both the reference ligand (RL 1) and reference drug (RD 1). Meanwhile, PES 1, PES 2, and PES 3 had binding affinities even lower than the other reference drug (RD 2), which implies that they can be possible candidates for better PARP1 inhibition.

CDK2 receptor (2A0C) binding affinities with the phytoecdysteroids were between -9.5 and -7.5 kcal mol^{-1}. Reference ligand (RL 2) binding affinity for the 8H7H receptor was -8.8 kcal mol^{-1}, whereas reference drugs (RD 3 and RD 4) binding affinities were -9.8 and -9.3 kcal mol^{-1}, respectively. The binding affinity of PES 12, PES 20, PES 6, PES 2, and PES 34 was equal to or less than that of one reference drug (RD 4) and reference ligand (RL 2) but greater than that of the other reference drug (RD 3), which show that they can be promising candidates for ABL1 inhibition.

ABL1 receptor (8H7H) binding affinities were between -10.0 and -7.0 kcal mol^{-1}. Reference ligand (RL 3) binding affinity for 2A0C receptor was -10.4 kcal mol^{-1}, whereas reference drugs (RD 5 and RD 6) binding affinities were -11.0 and -8.5 kcal mol^{-1}. The binding affinity of PES 10, PES 37, PES 25, PES 44, and PES 1 was lower than that of only one reference drug (RD 6) but greater than that of another reference drug (RD 5) and reference ligand (RL 3). Since these complexes have lower values than one of the reference drugs, they could be good candidates for CDK2 inhibition.

Table 2. Binding affinities of screened ligands against different receptors

Code	Binding affinity (kcal mol^{-1})		
	3L3M	**2A0C**	**8H7H**
PES 1	-11.3	-9.2	-9.1
PES 2	-11.2	-8.7	-8.6
PES 3	-10.9	-8.7	-8.3
PES 4	-10.8	-8.3	-8.3
PES 5	-10.4	-8.5	-7.8
PES 6	-10.3	-9.3	-9.0
PES 7	-10.3	-7.7	-7.5
PES 8	-10.2	-8.5	-9.0
PES 9	-10.2	-8.4	-8.2
PES 10	-10.2	-9.2	-10.0
PES 11	-10.2	-8.6	-8.9
PES 12	-10.1	-9.5	-8.6
PES 13	-10.1	-7.9	-7.3
PES 14	-10.1	-8.8	-7.7
PES 15	-10.1	-8.3	-9.0
PES 16	-10.1	-8.9	-8.6
PES 17	-10.1	-9.1	-7.8
PES 18	-10	-9.1	-9.0
PES 19	-9.9	8.9	-9.0
PES 20	-9.9	-9.4	-8.8
PES 21	-9.9	-8.8	-7.7
PES 22	-9.9	-8.5	-8.1
PES 23	-9.8	-8.0	-7.6

PES 24	-9.7	-7.9	-7.4
PES 25	-9.7	-8.3	-9.3
PES 26	-9.6	-8.4	-8.0
PES 27	-9.6	-7.7	-7.5
PES 28	-9.6	-7.9	-8.4
PES 29	-9.6	-8.8	-8.5
PES 30	-9.6	-8.9	-8.6
PES 31	-9.5	-9.0	-8.9
PES 32	-9.4	-7.9	-7.7
PES 33	-9.4	-8.8	-8.4
PES 34	-9.4	-9.3	-8.8
PES 35	-9.4	-9.0	-8.6
PES 36	-9.3	-8.4	-7.1
PES 37	-9.3	-9.0	-9.6
PES 38	-9.3	-8.5	-8.7
PES 39	-9.3	-8.3	-8.9
PES 40	-9.2	-7.7	-8.7
PES 41	-9.1	-8.3	-7.0
PES 42	-9	-7.5	-8.2
PES 43	-8.9	-7.5	-8.4
PES 44	9.5	-9.3	-9.2
RL 1	-10.1	-	-
RL 2	-	-8.8	-
RL 3	-	-	-10.4
RD 1	-10.3	-	-
RD 2	-10.8	-	-
RD 3	-	-9.8	-
RD 4	-	-9.3	-
RD 5	-	-	-11.0
RD 6	-	-	-8.5

Where RL and RD stand for reference ligand and reference drug.

RL 1: 2-{2-fluoro-4-[(2S)-piperidin-2-yl]phenyl}-1H-benzimidazole-7-carboxamide (pubchem CID: 46173035)

RL 2: Olomoucine II (pubchem CID: 5494414)

RL 3: Tozasertib (pubchem CID: 5494449)

RD 1: Niraparib (pubchem CID: 24958200)

RD 2: Talazoparib (pubchem CID: 135565082)

RD 3: Palbociclib (pubchem CID: 5330286)

RD 4: Dinaciclib (pubchem CID: 46926350)

RD 5: Imatinib (pubchem CID: 5291)

RD 6: Dasatinib (pubchem CID: 3062316)

Molecular-level details of protein-ligand interactions

Molecular-level details (2D and 3D structures of protein-ligand interactions) of the top ligand were visualised from the Biovia Discovery Studio Client 2021 program. Both 3D and 2D diagrams of these proteins were drawn for all three protein-ligand top complexes.

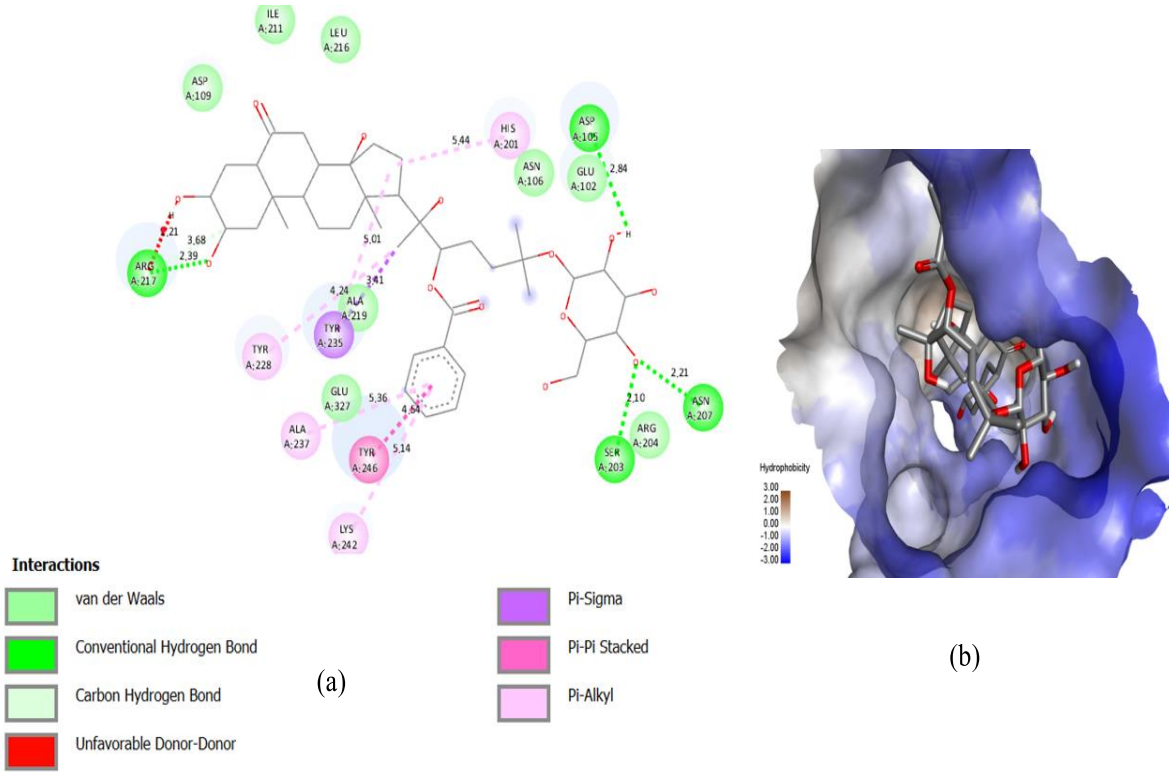

Figure 2. (a) 2D diagram of 3L3M having PES 1, (b) 3D diagram (Hydrophobicity surface) of 3L3M having PES 1

The protein shows both hydrogen bonds, van der Waals', and pi interactions. A hydrogen bond is present in ASP105, SER203, ASN207, and ARG217. The minimum distance required to form a hydrogen bond is 2.0 Å (Dannenberg, 1998). Van der Waals are present in ASN106, AP109, ARG204, ILE211, and LEU216. Pi interactions are present in HIS201, TYR228, ALA237, and TYR246. There are also some unfavourable bonds. Polar contact is the significant distance between polar amino acid residues and polar ligands. Polar contacts for the oxygen atom in the protein are at a distance of 2.1, 2.2, 2.4, 2.8, and 2.9 Å. Polar contacts for hydrogen atoms in ligands are at a distance of 2.2, 2.6, 2.8, 3.0, and 3.1 Å. These polar contacts have similar bond lengths to hydrogen bonds, as hydrogen bonds form between polar residues and ligands. The nearest neighbour is the distance between a selected atom and other atoms that are one bond away. A list consisting of all nearest neighbours is called the nearest neighbouring list. In the protein, significant distances between oxygen atoms and nearest neighbours are 3.1, 3.3, 3.5, and 3.9. For the hydrogen atom, the nearest neighbour distances are 3.0, 3.2, 3.3, 3.5, and 3.8 Å (Fig. 2a).

The hydrophobicity plot gives the relation between polarity and hydrophobicity between ligand and amino acid residues of the receptor. Polarity and hydrophobicity have an inverse interrelationship. The brown region of the receptor is a hydrophobic surface, whereas the blue region is a hydrophilic. The white region is between both surfaces. Protein shows mostly a blue region, which signifies that the surface has mostly a hydrophilic surface. It was due to polar amino acids like Arginine (ARG), Aspartate (ASP), Asparagine (ASN), Histidine (HIS), Serine (SER), and Tyrosine (TYR) (Fig. 2b).

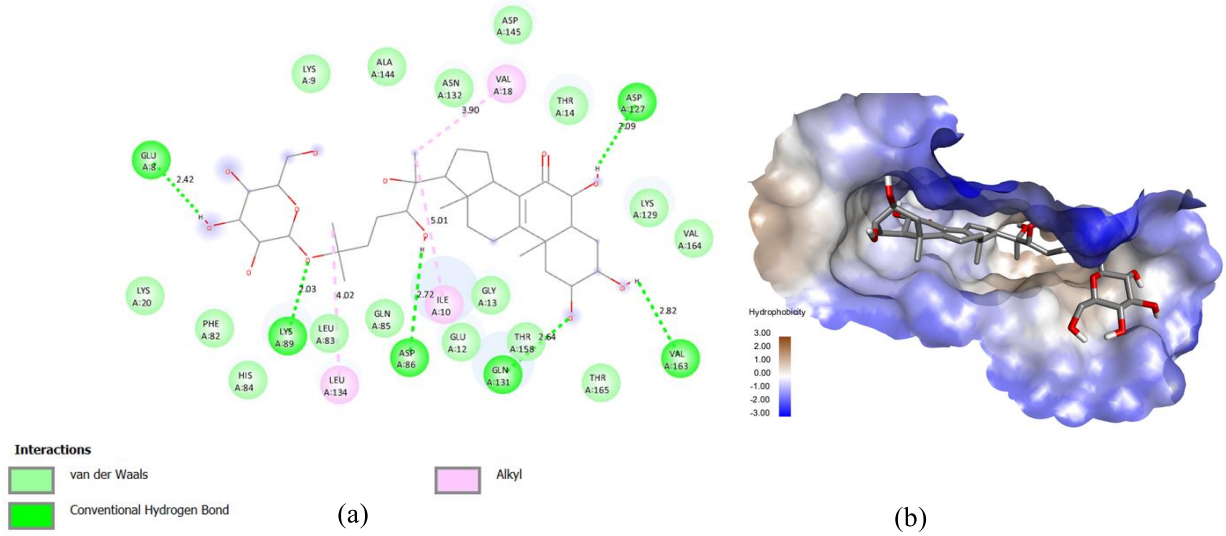

Figure 3. (a) 2D diagram of 2A0C having PES 12; (b) 3D diagram (Hydrophobicity) of 2A0C having PES 12

2A0C protein 2D shows hydrogen bond, van der Waals, and alkyl interaction. Hydrogen bond is present in GLU8, LYS89, ASP86, GLN131, ASP127 and VAL163. There are van der Waals' interactions present in LYS9, GLU12, THR14, PHE82, LEU83, HIS84, GLN85, ASN132, ALA144, ASP145, VAL164, and THR165. Alkyl interaction is present in ILE 10, VAL18, and LEU 134. Hydrogen bonding in the PES 5 was even better than the reference drug RD 4, as it had one more hydrogen bond. Polar contacts for the oxygen atom in the protein are at distances of 2.4, 2.6, 2.7, 2.8, and 2.9 Å. Polar contacts for the hydrogen atom in the ligand are at distances of 2.0, 2.7, 2.8, and 3.4 Å. These polar contacts have a similar bond length to hydrogen bonds, as hydrogen bonds form between polar residues and the ligand. In the protein, significant distances between the oxygen atom and its nearest neighbours are 3.3, 3.4, 3.5, and 3.8 Å. For the hydrogen atom, the nearest neighbour distances are 3.9, 4.0, 4.1, 4.3, and 4.4 Å (Fig. 3a).

The protein shows mostly blue colour as the surface is mostly hydrophilic. It is due to polar amino acids like Aspartate (ASP), Glutamate (GLU), Glutamine (GLN), and Lysine (LYS), which have electronegative atoms and make hydrogen bonds. The ligand binds distinctly in the polar region of the protein, as the surface is mostly hydrophilic. The protein surface shows mostly brownish white (Fig. 3b), which means the surface is a hydrophobic surface due to non-polar amino acids like Alanine (ALA), Leucine (LEU), and Valine (VAL).

The 2D surface interaction analysis of the 8H7H–PES10 complex reveals a network of hydrogen-bonding and hydrophobic contacts that contribute to ligand stabilization within the binding pocket. Two conventional hydrogen bonds are observed with GLY26 and ASP158, while multiple hydrophobic (alkyl) interactions are formed with LEU25, TYR30, LYS48, ILE90, and LEU147, indicating a strong affinity toward non-polar residues.

The polar contact map further supports these findings. The ligand forms oxygen-centered polar contacts with the protein at distances of 2.4, 2.6, and 2.8 Å, whereas hydrogen-centered polar interactions occur at 2.2, 3.3, 3.6, and 3.9 Å. These distances fall within the typical range reported for stabilizing polar or hydrogen-bond interactions, reinforcing the contribution of polar residues to ligand anchoring.

Examination of the protein environment shows that the oxygen atoms in the receptor maintain distances of 3.3, 3.4, 3.5, and 3.8 Å from their nearest neighboring atoms. For hydrogen atoms, the nearest-neighbor distances are 3.9, 4.2, 4.4, and 4.5 Å, consistent with additional weak polar or van der Waals contacts that complement the primary binding interactions (Fig 4a).

Figure 4.b illustrates the hydrophobicity-mapped surface of the 8H7H protein in complex with PES10. The surface is dominated by brownish-white regions, indicating a predominantly hydrophobic landscape enriched with non-polar amino acids such as Alanine (ALA), Leucine (LEU), Isoleucine (ILE), and Glycine (GLY). Although polar residues, including Aspartate (ASP), Lysine (LYS), and Tyrosine (TYR) are also present, their contribution is comparatively minor. The overall surface distribution confirms that PES10 primarily interacts with a hydrophobic binding channel, which aligns with the alkyl interaction profile observed in the docking analysis.

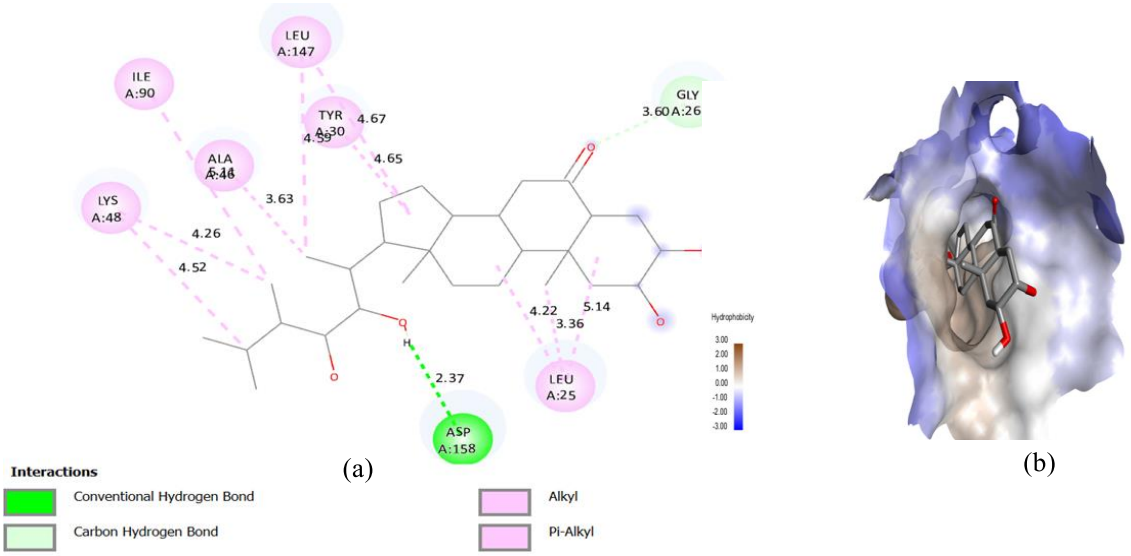

Figure 4. (a) 2D diagram of 8H7H having PES 10; (b) 3D (Hydrophobicity) diagram of 8H7H having PES 10

In-silico predictive cancer cell line inhibition study by the pdCSM server

The inhibitory anticancer activity of small ligands can be studied from the pdCSM server, which predicts these ligands' molecular pharmacodynamics and anticancer bioactivity against many cancer cell lines (groups of cancer cells that are derived from a single cancer cell). MDA-MD-468 (breast cancer), HCT-116 (colon cancer, CCRF (leukaemia), MDA-435 (melanoma), HOP-18 (non-small lung cancer), SK-OV-3 (ovarian cancer), DU-145 (prostate cancer), and SN12K1 (renal cancer) are different cancer cell lines. The table below shows the anticancer activity of hit candidates (top 5 candidates) against various cancer cell lines. The anticancer activity of the cell line is expressed in Growth Inhibition (GI_{50}), which is a log value (Table 3).

Table 3. Anticancer activity of hit candidates against the PARP1 protein (PDB ID: 3L3M) from the pdCSM server

S. N.	Code	Anticancer	Breast MDA-MB-468	Colon HCT-116	Leukaemia CCRF	Melanoma MDA-MB-435	Non-small HOP-18	Ovarian SK-OV-3	Prostate DU-145	Renal SN12K1
1	PES 1	Active	5.6	5.3	6.0	6.4	6.0	5.6	6.2	6.3
2	PES 2	Inactive	6.7	4.4	4.8	5.2	6.7	4.7	4.8	5.7
3	PES 3	Inactive	6.9	4.5	4.7	5.0	6.5	4.7	4.6	5.8
4	PES 4	Inactive	6.6	4.4	4.7	5.4	6.4	4.8	4.6	5.8
5	PES 5	Inactive	6.7	6.7	4.4	4.8	5.3	4.8	5.1	6.1
6	RL 1	Inactive	4.9	4.6	4.4	4.6	4.6	4.4	4.6	4.1
7	RD 1	Inactive	5.5	4.5	4.4	4.8	4.5	4.4	4.4	4.8
8	RD 2	Inactive	5.6	5.6	4.8	4.7	4.5	4.5	4.7	4.4

The pdCSM server shows the average anticancer activity of different cancers measured by the server. The anticancer values greater than 5 indicate activity towards specific cell lines. Though overall inhibitory anticancer activity of hit candidates (top 5) of 3L3M was inactive, they were active towards specific cancer cell lines. PES 1 was active against all cancer cell lines: MDA-MB-468, HCT-116, CCRF, MDA-MB-

435, HOP-18, SKOV3, DU145, and SN12K1. PES 27, PES 1, and PES 36 are active against only MDA-MB-468, MDA-435, HOP-18, DU-145, and SN12K1 cell lines. PES 5 was active against only MDA-MB-468, HCT-116, HOP-18, DU-145, and SN12K1 cell lines. Reference ligand or native ligand (RL 1) was inactive against all cell lines, which shows the hit candidates have greater pdCSM value anticancer properties than the native ligand. RD 1 was active only toward MDA-MB-468, and RD 2 is active only against MDA-MB-468 and HCT-116. Both reference drugs have a lower pdCSM overall value than the hit candidates. Since PES 1 was active against all cell lines, it can be a potent anticancer compound (Table 3).

Table 4. Anticancer activity of hit candidates against CDK2 protein (PDB ID: 2A0C) from the pdCSM server

S. N.	Code	Anticancer	Breast MDA-MD-468	Colon HCT-116	Leukaemia CCRF	Melanoma MDA-435	Non-small HOP-18	Ovarian SK-OV-3	Prostate DU-145	Renal SN12K1
1	PES 12	Inactive	6.8	4.4	4.7	5.1	6.5	4.7	4.7	5.7
2	PES 20	Inactive	6.7	5.0	5.1	5.4	5.4	5.5	4.8	5.3
3	PES 6	Inactive	6.8	4.4	4.6	4.8	5.5	4.8	4.7	4.8
4	PES 34	Inactive	6.9	5.2	5.9	6.5	5.4	5.4	6.2	6.7
5	PES 44	Inactive	6.8	5.2	6.0	6.4	6.0	5.6	6.2	6.4
6	RL 2	Inactive	5.8	5.0	4.6	4.9	4.4	4.4	4.8	4.7
7	RD 3	Inactive	5.5	4.8	4.6	5.1	4.5	4.5	5.1	4.6
8	RD 4	Inactive	5.7	5.0	4.5	5.1	4.3	4.6	5.0	4.8

PES 20 was active against all cancer cell lines except DU-145. PES 34 and PES 44 were active against all cell lines. PES 12 was active against all cell lines except SK-OV-3 and DU-145. PES 6 and RL 2 were active against only MDA468 and HOP-118 cell lines. RD 3 was active against only MDA468, MDA435, and DU-145 cell lines. RD 4 was active against MDA468, HCT-116, MDA435, and DU-145 cell lines, which shows that both reference drugs' anticancer properties were weaker than the hit candidates of 2A0C. PES 12, PES 20, PES 34, and PES 44 can be used as potent anticancer compounds as they are active against most cancer cell lines (Table 4).

Table 5. Anticancer activity of hit candidates against ABL1 protein (PDB ID: 8H7H) from the pdCSM server

S. N.	Code	Anticancer	Breast MDA-MB-468	Colon HCT-116	Leukaemia CCRF	Melanoma MDA-MB-435	Non-small HOP-18	Ovarian SK-OV-3	Prostate DU-145	Renal SN12K1
1	PES 10	Inactive	6.6	5.0	5.0	5.4	5.5	5.4	4.9	5.4
2	PES 37	Inactive	6.7	4.4	4.7	5.1	6.1	4.7	4.6	6.0
3	PES 25	Inactive	6.7	4.4	4.7	5.3	6.4	4.7	4.7	4.6
4	PES 44	Active	6.8	5.2	6.0	6.4	6.0	5.6	6.2	6.4
5	PES 1	Active	5.6	5.3	6.0	6.4	6.0	5.6	6.2	6.3
6	RL 3	Inactive	5.6	4.9	4.8	4.7	4.4	4.5	4.7	4.4
7	RD 5	Inactive	5.8	5.1	4.5	5.14	4.8	4.4	5.0	5.2
8	RD 6	Inactive	5.5	4.8	5.0	4.7	4.6	4.3	4.5	5.3

PES 10 was active against all cell lines except DU-145. PES 28 is active against all cell lines. PES 34 and PES 1 were active against MDA468, MDA435, HOP-18, and SN12K1. PES 25 was active against only MDA-MB-468, MDA-MB-435, and HOP-18. Native ligand (RL 3) is inactive towards all cell lines, which shows the better binding affinity with 8H7H receptor. RD 5 was active against MDA-MB-468, HCT-116,

MDA-MB-435, DU145, and SN12K1. RD 6 was active against only MDA-MB-468, MDA-MB-435, and SN12K1. Both reference drugs (RD 5 and RD 6) have lower anticancer properties than the hit candidates of 8H7H. PES 10 and PES 44 can be potent anticancer compounds as they were active towards most of the cell lines.

PES 1 can be used as a potent anticancer compound against the PARP1 receptor. PES 12, PES 20, PES 37, and PES 44 can be used as a potent anticancer compound against the CDK2 receptor. PES 10 and PES 44 can be used as potent anticancer compounds against the ABL1 receptor. PES 1 was found to exhibit anticancer activity against both PARP1 and ABL1 receptors. PES 44 was found to be effective against both CDK2 and ABL1 receptors. Similar results were obtained in a graph-based signature study with GI_{50} values < 5 μM showing action in breast, colon, leukaemia, and renal cancer cell lines. These results provide the validity of Table 5 (Neupane et al., 2024).

***In silico* predictive CDK2 inhibition study by the kinCSM server**

The kinCSM server predicts the anticancer activity of compounds against cyclin-dependent kinase protein (CDK2).

Table 6. CDK2 inhibition study of hit candidates against PARP1 protein (PDB ID: 3L3M) by the kinCSM server

S.N.	Code	CDK2 inhibitor (IC_{50} < 10 μM)	CDK2 ligand binding (pKi)	Allosteric or not	Type I or II	Type I1/2 or II	Type I or I1/2	Final decision
1	PES 1	No	5.801	No	I	I1/2	I	Type I
2	PES 2	No	5.907	No	I	I1/2	I	Type I
3	PES 3	No	5.871	No	I	I1/2	I	Type I
4	PES 4	No	5.883	No	I	I1/2	I	Type I
5	PES 5	No	5.811	No	I	I1/2	I	Type I
6	RL 1	Yes	5.300	No	I	II	I	Type I
7	RD 1	Yes	5.268	No	I	I1/2	I	Type I
8	RD 2	Yes	5.904	No	I	I1/2	I	Type I

None of the hit candidates inhibited CDK2, but both reference drugs, as well as reference ligands, inhibited CDK2, which shows the hit candidates are not good inhibitors against the CDK2 protein. All hit candidates, reference ligands, and reference drugs were of Type I. These inhibitors bind to the active site of the kinase. They compete with ATP for binding and are reversible. None of them inhibited at the allosteric site but inhibited at the orthosteric site of the protein (Table 6).

Table 7. CDK2 inhibition study of hit candidates against CDK2 protein (PDB ID: 2A0C) by the kinCSM server

S.N.	Code	CDK2 inhibitor (IC_{50} < 10 μM)	CDK2 ligand binding (pKi)	Allosteric or not	Type I or II	Type I1/2 or II	Type I or I1/2	Final decision
1	PES 12	No	5.901	No	I	I1/2	I	Type I
2	PES 20	No	5.862	No	I	I1/2	I	Type I
3	PES 6	Yes	5.859	No	I	I1/2	I	Type I
4	PES 34	No	5.877	No	I	I1/2	I	Type I
5	PES 44	No	5.801	No	I	I1/2	I	Type I
6	RL 2	Yes	5.169	No	I	I1/2	I	Type I
7	RD 3	No	5.149	No	I	II	I	Type I
8	RD 4	Yes	5.213	No	I	I1/2	I	Type I

PES 6, a native ligand (RL 2) and a reference drug (RD 4), inhibited CDK2 protein. All hit candidates and reference drugs inhibited the CDK2 protein. All hit candidates and reference drugs were of Type I. These inhibitors bind to the active site of the kinase. They compete with ATP for binding and are

reversible. None of them inhibited at the allosteric site, but inhibited at the orthosteric site of the protein. Hence, PES 12, PES 20, PES 6, PES 34, and PES 44 can be potent candidates against the CDK2 protein (Table 7), which were already justified by their binding affinity and pdCSM values.

Table 8. CDK2 inhibition study of hit candidates against ABL1 protein (PDB ID: 8H7H) by the kinCSM server

S.N.	Code	CDK2 inhibitor (IC_{50} < 10 µM)	CDK2 ligand binding (pKi)	Allosteric or not	Type I or II	Type I1/2 or II	Type I or I1/2	Final decision
1	PES 10	No	5.872	No	I	I1/2	I	Type I
2	PES 37	No	5.876	No	I	I1/2	I	Type I
3	PES 25	No	5.855	No	I	I1/2	I	Type I
4	PES 44	No	5.877	No	I	I1/2	I	Type I
5	PES 1	No	5.887	No	I	I1/2	I	Type I
6	RL 3	Yes	6.807	No	I	I1/2	I1/2	Type I1/2
7	RD 5	No	6.029	No	I	I1/2	I	Type I
8	RD 6	Yes	5.693	No	I	I1/2	I	Type I

None of the hit candidates and a reference drug, RD3, inhibited CDK2. A reference ligand (RL 3) and a reference drug (RD 6) inhibited CDK2. All hit candidates and reference drugs were of Type I, except the native ligand (RL2), which was of Type I1/2. Type I inhibitors bind to the active site of the kinase. They compete with ATP for binding and are reversible. Type I1/2 can bind to the active site with or without displacing the DFG motif (Asp-Phe-Gly). They are also reversible. None of them inhibited at the allosteric site but inhibited at the orthosteric site of the protein. This shows the hit candidates are not good inhibitors against the CDK2 protein.

Only PES 6 was a good inhibitor against the CDK2 receptor. There were similar results in a study that showed CDK2 inhibitors had IC_{50} values greater than 10 µM with a type I non-allosteric binding mode (Table 8) (Neupane et al., 2024).

***In-silico* predictive ADMET study by the ADMETlab2.0 server**

ADMETlab2.0 server predicts the physicochemical, pharmacokinetics, and pharmacodynamics properties of compounds. Major physicochemical parameter includes water solubility (Log S), whereas major pharmacokinetics parameters include human intestinal absorption (HIA), blood-brain-barrier (BBB), plasma protein binding (PBB), CYP2D6-inhibitor, CYP2D6-substrate, and clearance (CL). Human Ether-à-go-go-Related gene (hERG), drug-induced liver injury (DILI), rat oral acute toxicity (ROA), skin sensitivity, carcinogenicity, effective concentration (EC), effective inhibition (EI), and respiratory are major parameters of pharmacodynamics. There are two types of tables for ADMET prediction of hit candidates for each receptor. One table shows the physicochemical and pharmacokinetic values of hit candidates, whereas another table shows the pharmacodynamic values of hit candidates of each receptor. The table shows the probability of the particular parameter activity.

Table 9. Physicochemical and pharmacokinetic activity of hit candidates against PARP1 protein (PDB ID: 3L3M)

S. N.	Code	Log S Log (mol/L)	HIA (% absorbed)	BBB (cm/s)	PPB (% bound)	CYP2D6-inhibitor	CYP2D6-substrate	CL [Log (mL/min/Kg)]
	Optimum range	-4 to 0.5	0 to 70 %	0 to 0.7	0 to 90%	0 to 0.7	0 to 0.7	0 to 0.5
1	PES 1	-3.3	87.8%	0.1	73.1%	0.0	0.1	1.5
2	PES 2	-3.0	67.2%	0.1	85.7%	0.0	0.1	1.5
3	PES 3	-2.9	47.0%	0.1	55.1%	0.0	0.0	2.3
4	PES 4	-2.9	91.9%	0.1	41.8%	0.0	0.0	1.1

5	PES 5	-4.4	0.7%	0.2	87.4%	0.0	0.6	6.9
6	RL 1	-4.1	0.4%	0.6	90.3%	0.8	0.8	4.0
7	RD 1	-3.1	0.8%	0.9	90.2%	0.8	0.8	6.8
8	RD 2	-4.5	2.6%	0.0	95.6%	0.0	0.2	5.7

All hit candidates of the 3L3M receptor, reference ligand (RL 1), and reference drugs (RD 1 and RD 2) had logarithmic solubility in an optimum range. Human intestinal absorption (HIA) was also found to be in the optimum range, except for PES 1. Blood-brain barrier (BBB), plasma protein binding permeation (PPB), CYP2D6 inhibitor, and CYP2D6 substrate were in the optimum range for all hit candidates. Clearance for all hit candidates, including RL 1, RD 1, and RD 2, was higher than the optimum range of 0.5 mL min^{-1} kg^{-1}. High total clearance affects drug exposure, dosing requirements, and therapeutic outcomes (Table 9).

Table 10. Pharmacodynamics activity of hit candidates against PARP1 protein (PDB ID: 3L3M)

S.N.	Code	hERG	DILI	ROA	Skin sensitivity	Carcinogenicity	EC	EI	Respiratory
	Optimum range	0 to 0.7	0 to 0.7	0 to 0.7	0 to 0.7	0 to 0.7	0 to 0.7	0 to 0.7	0 to 0.7
1	PES 1	0.1	0.1	0.0	0.0	0.0	0.0	0.0	0.7
2	PES 2	0.0	0.0	0.2	0.0	0.0	0.0	0.0	0.8
3	PES 3	0.0	0.0	0.2	0.2	0.4	0.0	0.0	0.9
4	PES 4	0.0	0.0	0.4	0.1	0.0	0.0	0.0	0.9
5	PES 5	0.2	0.3	0.1	0.2	0.5	0.0	0.0	0.9
6	RL 1	0.8	0.7	0.9	0.0	0.2	0.0	0.0	0.9
7	RD 1	0.9	0.9	0.7	0.1	0.1	0.0	0.0	0.7
8	RD 2	0.5	0.9	0.7	0.2	0.8	0.0	0.0	0.9

All hit candidates had an optimum activity of human ether-a-go-go gene blocker (hERG), drug-induced liver injury (DILI), rat oral activity (ROA), carcinogenicity, eye corrosion (EC), and eye irritation (EI), which were similar to the activity of reference ligand (RL 1) and reference drugs (RD 1 and RD 2). But hit candidates, reference ligand, and reference drugs had higher activity than optimum respiratory toxicity, which poses significant risks to lungs health and overall well-being. PES 1, PES 2, PES 3, PES 4, and PES 5 can be used as potent anticancer compounds against PARP1 receptors (Table 10).

Table 11. Physicochemical and pharmacokinetic activity of hit candidates against CDK2 protein (PDB ID: 2A0C)

S.N.	Code	Log S Log (mol/L)	HIA (% absorbed)	BBB (cm/s)	PPB (% bound)	CYP2D6-inh	CYP2D6-sub	CL Log [(mL/min/Kg)]
	Optimum range	-4 to 0.5	0 to 70%	0 to 0.7	0 to 90%	0 to 0.7	0 to 0.7	0 to 0.5
1	PES 12	-3.	79.8%	0.1	074.5%	0.0	0.0	1.8
2	PES 20	-3.7	48.5%	0.0	88.5%	0.0	0.0	1.1
3	PES 6	-3.0	81.3%	0.1	69.9%	0.0	0.1	2.2
4	PES 34	-3.5	77.8%	0.1	76.9%	0.0	0.0	1.5
5	PES 44	-3.3	87.8%	0.1	73.1%	0.0	0.1	1.5
6	RL 2	-3.7	14.%	0.9	96.7%	0.4	0.9	2.5
7	RD 3	-3.2	72.%	0.9	90.3%	0.2	0.8	8.2
8	RD 4	-4.2	0.5%	0.8	93.9%	0.6	0.8	2.7

All hit candidates of the 2A0C receptor had optimum activity against HIA, CYP2D6 inhibitor, and CYP2D6 substrate, which had similar activity as the reference ligand and drugs. All hit candidates, reference ligand (RL 2), and reference drugs (RD 3 and RD 4) had higher activity than optimum activity against total clearance, affecting drug exposure, dosing requirements, and therapeutic outcomes (Table 11).

Table 12. Pharmacodynamics activity of hit candidates against CDK2 protein (PDB ID: 2A0C)

S.N.	Code	hERG	DILI	ROA	Skin sensitivity	Carcinogenicity	EC	EI	Respiratory
	Optimum range	0 to 0.7	0 to 0.7	0 to 0.7	0 to 0.7	0 to 0.7	0 to 0.7	0 to 0.7	0 to 0.7
1	PES 12	0.0	0.1	0.0	0.0	0.0	0.0	0.0	0.8
2	PES 20	0.0	0.1	0.8	0.0	0.1	0.0	0.0	0.8
3	PES 6	0.1	0.0	0.1	0.1	0.0	0.0	0.0	0.0
4	PES 34	0.1	0.0	0.1	0.2	0.0	0.0	0.0	0.8
5	PES 44	0.1	0.1	0.0	0.0	0.0	0.0	0.0	0.7
6	RL 2	0.6	0.9	0.0	0.1	0.8	0.0	0.0	0.9
7	RD 3	0.9	0.9	0.6	0.9	0.0	0.0	0.0	0.9
8	RD 4	0.8	0.9	0.7	0.1	0.9	0.0	0.0	0.8

All hit candidates had optimum activity against hERG, DILI, ROA, skin sensitivity, carcinogenicity, EC, and EI, which had similar activity as reference ligand (RL 2) and reference drugs (RD 3 and RD 4). The hit candidates, reference ligand, and reference drugs had higher activity than optimum activity against respiratory toxicity, which poses significant risks to lungs health and overall well-being. Thus, PES 12, PES 20, PES 6, PES 34, and PES 44 can be used as potent anticancer compounds against the CDK2 receptor (Table 12).

All hit candidates of the 8H7H receptor had optimum activity against HIA, CYP2D6 inhibitor, and CYP2D6 substrate, which had similar activity to the reference ligand and reference drugs. The hit candidates, reference ligand (RL 3), and reference drugs (RD 5 and RD 6) had higher activity than the optimum range against the clearance (CL), which affects drug exposure, dosing requirements, and therapeutic outcomes (Table 13).

Table 13. Physicochemical and pharmacokinetic values of hit candidates against ABL1 protein (PDB ID: 8H7H)

S. N.	Code	Log S Log (mol/L)	HIA (% absorbed)	BBB permeability (cm/s)	PPB (% bound)	CYP2D6-inhibitor	CYP2D6-substrate	CL Log [(mL/min/Kg)]
	Optimum range	-4 to 0.5	0 to 0.7	0 to 0.7	0 to 0.9	0 to 0.7	0 to 0.7	0 to 0.5
1	PES 10	-4.0	88.2%	0.1	76.9%	0.0	0.1	1.6
2	PES 37	-3.1	91.2%	0.1	50.5%	0.0	0.0	1.3
3	PES 25	-3.0	88.4%	0.1	47.9%	0.0	0.0	1.7
4	PES 44	-3.5	77.8%	0.1	76.8%	0.0	0.0	1.5
5	PES 1	-2.9	87.7%	0.1	73.4%	0.0	0.0	1.5
6	RL 3	-2.5	49.2%	0.5	29.5%	0.0	0.0	10.5
7	RD 5	-3.3	0.7%	0.5	69.4%	0.1	0.1	3.7
8	RD 6	-3.0	2.3%	0.3	39.3%	0.6	0.0	10.1

Table 14. Pharmacodynamics activity of hit candidates against ABL1 protein (PDB ID: 8H7H)

S.N.	Code	hERG	DILI	ROA	Skin Sensitivity	Carcinogenicity	EC	EI	Respiratory
	Optimum range	0 to 0.7	0 to 0.7	0 to 0.7	0 to 0.7	0 to 0.7	0 to 0.7	0 to 0.7	0 to 0.7
1	PES 10	0.1	0.2	0.7	0.2	0.0	0.0	0.0	0.4
2	PES 37	0.1	0.0	0.2	0.2	0.0	0.0	0.01	1.0
3	PES 25	0.1	0.0	0.6	0.3	0.1	0.0	0.0	0.9
4	PES 44	0.1	0.1	0.2	0.2	0.1	0.0	0.0	0.9
5	PES 1	0.1	0.1	0.3	0.2	0.1	0.0	0.0	0.9
6	RL 3	0.2	0.9	0.9	0.5	0.8	0.0	0.0	1.0
7	RD 5	0.8	1.0	0.6	0.9	0.8	0.0	0.0	0.9
8	RD 6	0.2	0.0	0.0	0.9	0.1	0.0	0.0	0.9

All hit candidates had optimum activity except hERG, DILI, ROA, skin sensitivity, carcinogenicity, EC, and EI, which had similar activity as reference ligands and reference drugs. The hit candidates, reference ligand (RL 3), and reference drugs (RD 5 and RD 6) had higher activity than optimum activity against the respiratory which poses significant risks to lungs health and overall well-being. Thus, PES 10, PES 37, PES 25, PES 44, and PES 1 (Fig. 5) can be used as potent anticancer compounds against the ABL1 receptor (Table 14).

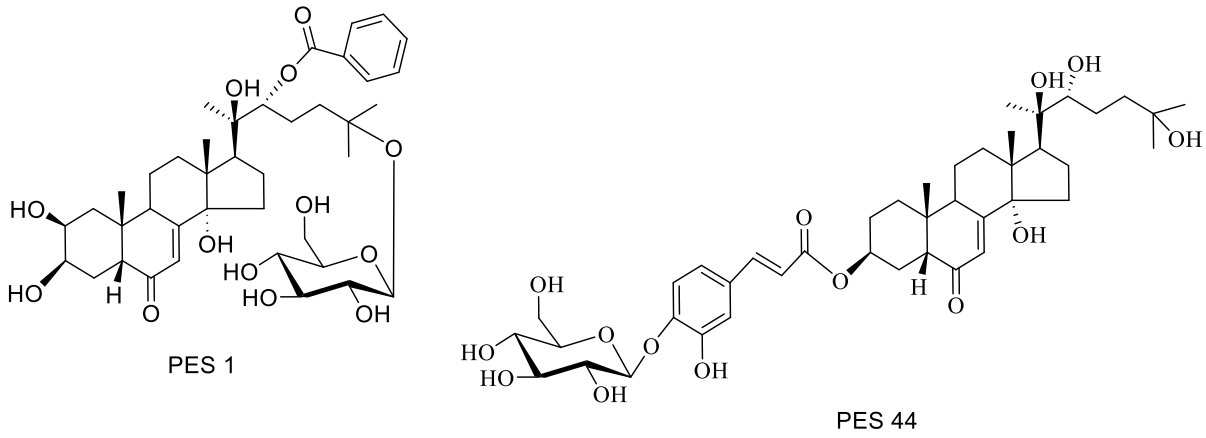

Figure 5. Structure of phytoecdysteroids with potent anticancer activity

CONCLUSION

Molecular docking of ligands with 3L3M showed PES 1 and PES 2 to have the highest binding affinities; 2A0C showed PES 12 and PES 20 to have the highest binding affinities. The 3D diagrams of the three proteins showed the predominant hydrophobic surface region in 3L3M having PES 1, 2A0C having PES 20, 8H7H having PES 10, and 8H7H having PES 37; the predominant hydrophilic surface region in 3L3M having PES 2 and 2A0C having PES 12. 2D diagrams of the three proteins had hydrogen bonding within 2.1 to 3.3 Å. Polar contacts were also within 2.0 to 3.5 Å, and nearest neighbours were between 2.5 and 5.0 Å. PES 1 was found to exhibit anticancer activity against both PARP1 and ABL1 receptors. PES 44 was found to be effective against both CDK2 and ABL1 receptors. Hence, PES 1 and PES 44 are potent compounds that can be used for *in vivo* and *in vitro* tests. These two compounds are the findings of this study, and this is important for the future study of cancer inhibitors targeting PARP1 & CDK2.

ACKNOWLEDGMENTS

The authors are grateful to the Central Department of Chemistry, Kirtipur, Kathmandu (Tribhuvan

University), for providing research facilities in pursuing this work.

AUTHORS CONTRIBUTION

Conceptualization: JA, AA; Methodology: NM, AP, AW; Validation: AA, JA; Investigation: NM, ARP, AW; Data analysis: NM, AP, ARP, NB, AW; Writing-original draft: NM, AP, ARP, AA; Writing-review & editing: AA; Supervision: JA

FUNDING

None

ORCIDs

Nitesh Mallik:
https://orcid.org/0000-0003-3478-8484
Ashish Phuyal:
https://orcid.org/0009-0000-6126-0023
Anuraj Phunyal:
https://orcid.org/0009-0007-6739-3071
Narendra Bhatta:
https://orcid.org/0009-0002-1316-3848
Amar Waiba:
https://orcid.org/0009-0005-5783-5089
Jhashanath Adhikari Subin:
https://orcid.org/0000-0001-8515-9843
Achyut Adhikari:
https://orcid.org/0000-0002-1065-5727

CONFLICT OF INTEREST

The authors declare that there are no conflicts of interest regarding the publication of this article.

DATA AVAILABILITY STATEMENT

The data that support the findings of this study are available from the corresponding author upon reasonable request.

SUPPLEMENTARY INFORMATION

Table S1: List of phytoecdysteroids selected for molecular docking calculations, Figure S2: Molecular structure of screened phytoecdysteroid, Table S2: Ramachandran plot analysis of different receptors, Fig S2: Ramchandran plot of 3L3M receptor, Fig S3: Ramchandran plot of 2A0C receptor, Fig S4: Ramchandran plot of 8H7H, Table S3: Toxicity results from PRO-tox II server

REFERENCES

Adhikari, B., Phuyal, A., Phunyal, A., Upadhyaya, N., Waiba, A., & Adhikari, A. (2025). In silico exploration of potent phytoecdysteroids targeting multiple receptors in non-small cell lung cancer. *Journal of Nepal Chemical Society*, *45*(1), 143–155. https://doi.org/10.3126/jncs.v45i1.74494

Al-Jarf, R., de Sá, A. G. C., Pires, D. E. V., & Ascher, D. B. (2021). pdCSM-cancer: Using graph-based signatures to identify small molecules with anticancer properties. *Journal of Chemical Information and Modeling*, *61*(7), 3314–3322. https://doi.org/10.1021/acs.jcim.1c00168

Altschul, S. F., Madden, T. L., Schäffer, A. A., Zhang, J., Zhang, Z., Miller, W., & Lipman, D. J. (1997). Gapped BLAST and PSI-BLAST: A new generation of protein database search programs. *Nucleic Acids Research*, *25*(17), 3389–3402. doi: 10.1093/nar/25.17.3389.

Asghar, U., Witkiewicz, A. K., Turner, N. C., & Knudsen, E. S. (2015). The history and future of targeting cyclin-dependent kinases in cancer therapy. *Nature Reviews Drug Discovery*, *14*(2), 130–146. https://doi.org/10.1038/nrd4504

Banerjee, P., Eckert, A. O., Schrey, A. K., & Preissner, R. (2018). ProTox-II: A webserver for the prediction of toxicity of chemicals. *Nucleic Acids Research*, *46*(W1), W257–W263. https://doi.org/10.1093/nar/gky318

Baskar, R., Lee, K. A., Yeo, R., & Yeoh, K.-W. (2012). Cancer and radiation therapy: current advances and future directions. *International Journal of Medical Sciences*, *9*(3), 193–199. https://doi.org/10.7150/ijms.3635

Bathori, M., & Pongracz, Z. (2005). Phytoecdysteroids–from isolation to their effects on humans. *Current Medicinal Chemistry*, *12*(2), 153–172. https://doi.org/10.2174/0929867053363450

Biasini, M., Schmidt, T., Bienert, S., Mariani, V., Studer, G., Haas, J., … Schwede, T. (2013). OpenStructure: An integrated software framework for computational structural biology. *Acta Crystallographica Section D: Biological Crystallography*, *69*(5), 701–709. https://doi.org/10.1107/S0907444913007051

Biasini, M., Bienert, S., Waterhouse, A., Arnold, K., Studer, G., Schmidt, T., … Schwede, T. (2014). SWISS-MODEL: Modelling protein tertiary and quaternary structure using evolutionary information. *Nucleic Acids Research*, *42*. https://doi.org/10.1093/nar/gku340

Bowie, J. U., Lüthy, R., & Eisenberg, D. (1991). A method to identify protein sequences that fold into a known three-dimensional structure. *Science (New York, N.Y.)*, *253*(5016), 164–170. https://doi.org/10.1126/science.1853201

Brown, J. S., Amend, S. R., Austin, R. H., Gatenby, R. A., Hammarlund, E. U., & Pienta, K. J. (2023). Updating the definition of cancer. *Molecular Cancer Research*, *21*(11), 1142–1147.

https://doi.org/10.1158/1541-7786.MCR-23-0411

Chen, P., Tang, G., Zhu, C., Sun, J., Wang, X., Xiang, M., … Yao, S. Q. (2023). 2-Ethynylbenzaldehyde-based, lysine-targeting irreversible covalent inhibitors for protein kinases and nonkinases. *Journal of the American Chemical Society*, *145*(7), 3844–3849. https://doi.org/10.1021/jacs.2c11595

Chhikara, B. S., & Parang, K. (2023). Global cancer statistics 2022: the trends projection analysis. *Chemical Biology Letters*, *10*(1), 451–451. https://scholar.google.com/scholar?q=urn:nbn:sciencein.cbl.2023.v10.451

Chiang, L.-C., Ng, L. T., Chiang, W., Chang, M.-Y., & Lin, C.-C. (2003). Thieme e-journals-planta medica. Retrieved September 2, 2023, from https://www.thieme-connect.com/products/ejournals/abstract/10.1055/s-2003-41113

Colovos, C., & Yeates, T. O. (1993). Verification of protein structures: Patterns of nonbonded atomic interactions. *Protein Science*, *2*(9), 1511–1519. https://doi.org/10.1002/pro.5560020916

Dannenberg, J. J. (1998). An introduction to hydrogen bonding by George A. Jeffrey (University of Pittsburgh). Oxford University Press: New York and Oxford. 1997. ix + 303 pp. $60.00. ISBN 0-19-509549-9. *Journal of the American Chemical Society*, *120*(22), 5604–5604. https://doi.org/10.1021/ja9756331

Das, N., Mishra, S. K., Bishayee, A., Ali, E. S., & Bishayee, A. (2021). The phytochemical, biological, and medicinal attributes of phytoecdysteroids: An updated review. *Acta Pharmaceutica Sinica B*, *11*(7), 1740–1766. https://doi.org/10.1016/j.apsb.2020.10.012

Hanwell, M. D., Curtis, D. E., Lonie, D. C., Vandermeersch, T., Zurek, E., & Hutchison, G. R. (2012). Avogadro: An advanced semantic chemical editor, visualization, and analysis platform. *Journal of Cheminformatics*, *4*(1), 17. https://doi.org/10.1186/1758-2946-4-17

Hoelder, S., Clarke, P. A., & Workman, P. (2012). Discovery of small molecule cancer drugs: Successes, challenges and opportunities. *Molecular Oncology*, *6*(2), 155–176. https://doi.org/10.1016/j.molonc.2012.02.004

Karki, D., Phunyal, A., & Adhikari, A. (2024). Estimation of total phenolic content, total flavonoid content, anti-oxidant activity and molecular docking studies of *Stereocaulon piluliferum* Th. *Journal of Plant Resources*, *22*(1), 104–112. https://doi.org/10.3126/bdpr.v22i1.68351

Khatiwada, R., Shrestha, A., Gyawali, K., Upadhyaya, S. R., Pradhan, R., Phuyal, A., … Parajuli, N. (2025). In-Silico analysis of secondary metabolites that inhibit aldose reductase targeting diabetic retinopathy. *Journal of Institute of Science and Technology*, *30*(1), 197–209. https://doi.org/10.3126/jist.v30i1.76562

Klijn, C., Durinck, S., Stawiski, E. W., Haverty, P. M., Jiang, Z., Liu, H., … Zhang, Z. (2015). A comprehensive transcriptional portrait of human cancer cell lines. *Nature Biotechnology*, *33*(3), 306–312. https://doi.org/10.1038/nbt.3080

Kryštof, V., McNae, I. W., Walkinshaw, M. D., Fischer, P. M., Müller, P., Vojtěšek, B., … Strnad, M. (2005). Antiproliferative activity of olomoucine II, a novel 2,6,9-trisubstituted purine cyclin-dependent kinase inhibitor. *Cellular and Molecular Life Sciences CMLS*, *62*(15), 1763–1771. https://doi.org/10.1007/s00018-005-5185-1

Laskowski, R. A., MacArthur, M. W., Moss, D. S., & Thornton, J. M. (1993). PROCHECK: A program to check the stereochemical quality of protein structures. *Journal of Applied Crystallography*, *26*(2), 283–291. https://doi.org/10.1107/S0021889892009944

Laskowski, R. A., Furnham, N., & Thornton, J. M. (2012). The Ramachandran plot and protein structure validation. In *Biomolecular Forms and Functions* (pp. 62–75). https://doi.org/10.1142/9789814449144_0005

Malhotra, V., & Perry, M. C. (2003). Classical chemotherapy: mechanisms, toxicities and the therapeutc window. *Cancer Biology & Therapy*, *2*(sup1), 1–3. https://doi.org/10.4161/cbt.199

Neupane, P., Adhikari Subin, J., & Adhikari, R. (2024). Assessment of iridoids and their similar structures as antineoplastic drugs by in silico approach. *Journal of Biomolecular Structure & Dynamics*, 1–16. https://doi.org/10.1080/07391102.2024.2314262

Nussbaumer, S., Bonnabry, P., Veuthey, J.-L., & Fleury-Souverain, S. (2011). Analysis of anticancer drugs: A review. *Talanta*, *85*(5), 2265–2289. https://doi.org/10.1016/j.talanta.2011.08.034

Palazzo, L., & Ahel, I. (2018). PARPs in genome stability and signal transduction: Implications for cancer therapy. *Biochemical Society Transactions*, *46*(6), 1681–1695. https://doi.org/10.1042/BST20180418

Penning, T. D., Zhu, G.-D., Gong, J., Thomas, S., Gandhi, V. B., Liu, X., … Giranda, V. L. (2010). Optimization of phenyl-substituted benzimidazole carboxamide poly(ADP-Ribose)

polymerase inhibitors: identification of (S)-2-(2-Fluoro-4-(pyrrolidin-2-yl)phenyl)-1H-benzimidazole-4-carboxamide (A-966492), a highly potent and efficacious inhibitor. *Journal of Medicinal Chemistry*, *53*(8), 3142–3153. https://doi.org/10.1021/jm901775y

Philipp-Staheli, J., Payne, S. R., & Kemp, C. J. (2001). p27Kip1: Regulation and Function of a Haploinsufficient Tumor Suppressor and Its Misregulation in Cancer. *Experimental Cell Research*, *264*(1), 148–168. https://doi.org/10.1006/excr.2000.5143

Phuyal, A., Ojha, P. K., Guragain, B., & Chaudhary, N. K. (2019). Phytochemical screening, metal concentration determination, antioxidant activity, and antibacterial evaluation of D*rymaria diandra* plant. *Beni-Suef University Journal of Basic and Applied Sciences*, *8*(1), 16. https://doi.org/10.1186/s43088-019-0020-1

Raimondi, C., Fantin, A., Lampropoulou, A., Denti, L., Chikh, A., & Ruhrberg, C. (2014). Imatinib inhibits VEGF-independent angiogenesis by targeting neuropilin 1–dependent ABL1 activation in endothelial cells. *Journal of Experimental Medicine*, *211*(6), 1167–1183. https://doi.org/10.1084/jem.20132330

Rose, P. W., Prlić, A., Altunkaya, A., Bi, C., Bradley, A. R., Christie, C. H., … Burley, S. K. (2017). The RCSB protein data bank: Integrative view of protein, gene and 3D structural information. *Nucleic Acids Research*, *45*(D1), D271–D281. https://doi.org/10.1093/nar/gkw1000

Roskoski, R. (2014). The ErbB/HER family of protein-tyrosine kinases and cancer. *Pharmacological Research*, *79*, 34–74. https://doi.org/10.1016/j.phrs.2013.11.002

Roskoski, R. (2016). Classification of small molecule protein kinase inhibitors based upon the structures of their drug-enzyme complexes. *Pharmacological Research*, *103*, 26–48. https://doi.org/10.1016/j.phrs.2015.10.021

Schott, A. F., Perou, C. M., & Hayes, D. F. (2015). Genome medicine in cancer: what's in a name? *Cancer Research*, *75*(10), 1930–1935. https://doi.org/10.1158/0008-5472.CAN-15-0174

Schrodinger, L., & Delano, W. (2020). PyMOL | pymol.org. Retrieved September 19, 2023, from https://pymol.org/2/

Seebacher, N. A., Stacy, A. E., Porter, G. M., & Merlot, A. M. (2019). Clinical development of targeted and immune based anti-cancer therapies. *Journal of Experimental & Clinical Cancer Research*, *38*(1), 156. https://doi.org/10.1186/s13046-019-1094-2

Trott, O., & Olson, A. J. (2010). AutoDock Vina: Improving the speed and accuracy of docking with a new scoring function, efficient optimization, and multithreading. *Journal of Computational Chemistry*, *31*(2), 455–461. https://doi.org/10.1002/jcc.21334

Waiba, A., Phunyal, A., Lamichhane, T. R., Ghimire, M. P., Nyaupane, H., Phuyal, A., & Adhikari, A. (2025). Computational insights into flavonoids inhibition of dengue virus envelope protein: ADMET profiling, molecular docking, dynamics, PCA, and end-state free energy calculations. *PLOS ONE*, *20*(7), e0327862. https://doi.org/10.1371/journal.pone.0327862

Waterhouse, A., Bertoni, M., Bienert, S., Studer, G., Tauriello, G., Gumienny, R., … Schwede, T. (2018). SWISS-MODEL: Homology modelling of protein structures and complexes. *Nucleic Acids Research*, *46*(W1), W296–W303. https://doi.org/10.1093/nar/gky427

Zhou, Y., Lih, T. M., Pan, J., Höti, N., Dong, M., Cao, L., … Li, Q. K. (2020). Proteomic signatures of 16 major types of human cancer reveal universal and cancer-type-specific proteins for the identification of potential therapeutic targets. *Journal of Hematology & Oncology*, *13*(1), 170. https://doi.org/10.1186/s13045-020-01013-x